Automated Retinal Lesion Detection via Image Saliency Analysis

Yitian Zhao[1*], Qifeng Yan[1], Yalin Zheng[1,2], Yonghuai Liu[3], Kang Zhou[1,4], Alejandro Frangi[1,5], Jiang Liu[1,6]

1 Cixi Institute of Biomedical Engineering, Ningbo Institute of Industrial Technology, Chinese Academy of Sciences, China.

2 Department of Eye and Vision Science, University of Liverpool, UK

3 Department of Computer Science, Edge Hill University, UK

4 School of Information Science and Technology, ShanghaiTech University, China.

5 School of Computing, University of Leeds, China.

6 Department of Computer Science and Engineering, Southern University of Science and Technology, China.

∗ E-mail: yitian.zhao@nimte.ac.cn

Abstract

Background and Objective: The detection of abnormalities such as lesions or leakage from retinal images is an important health informatics task for automated early diagnosis of diabetic and malarial retinopathy or other eye diseases, in order to prevent blindness and common systematic conditions. In this work, we propose a novel retinal lesion detection method by adapting the concepts of saliency. **Methods:** Retinal images are firstly segmented as superpixels, two new saliency feature representations: *uniqueness* and *compactness*, are then derived to represent the superpixels. The pixel level saliency is then estimated from these superpixel saliency values via a bilateral filter. These extracted saliency features form a matrix for low-rank analysis to achieve saliency detection. The precise contour of a lesion is finally extracted from the generated saliency map after removing confounding structures such as blood vessels, the optic disc, and the fovea. The main novelty of this method is that it is an effective tool for detecting different abnormalities at pixel-level from different modalities of retinal images, without the need to tune parameters. **Results:** To evaluate its effectiveness, we have applied our method to seven public datasets of diabetic and malarial retinopathy with four different types of lesions: exudate, hemorrhage, microaneurysms, and leakage. The evaluation was undertaken at pixel-level, lesion-level, or image-level according to ground truth availability in these datasets. **Conclusions:** The experimental results show that the proposed

method outperforms existing state-of-the-art ones in applicability, effectiveness, and accuracy.

Keywords: Saliency, feature, low-rank, retinal image, lesion detection

1 Introduction

The human retina is a window that allows clinicians to study retinal conditions such as diabetic retinopathy (DR) [1] and malarial retinopathy (MR) [2] as well as other systematic conditions such as cardiovascular diseases and stroke with non-invasive imaging techniques due to its transparency in nature. In particular, DR is a leading cause of vision impairment and loss in the working-age population [3] which affects nearly 500 million of people with diabetes worldwide. The severity of DR is usually determined by identifying specific features, such as exudates (EX), microaneurysms (MA), and hemorrhages (HE) in retinal color fundus (CF) images. MR has been identified as an important clinical sign in the diagnosis and prognosis of cerebral malaria (CM), which is still a major cause of death and disability in children in sub-Saharan Africa. Leakage (LK) in fluorescein angiogram (FA) is an important sign in determining the activity and development of lesions of MR [2]. Figure 1 shows these four types of anomalies in MR and DR respectively. The automated detection of these pathologies from retinal images is important in understanding the mechanism, diagnosis, optimal treatment and surgical planning in tackling retinal diseases.

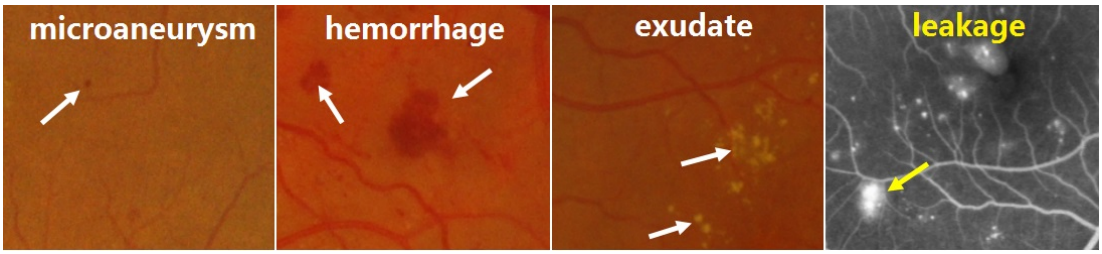

Figure 1: Four types of retinal abnormalities in color fundus and fluorescein angiography respectively.

Current practical approaches for the quantitative analysis of retinal abnormalities require extensive manual annotation by experienced graders [4]. Manual grading is often time-consuming, expensive and subject to human errors, thus will be impractical for routine clinical applications. To overcome these limitations, cost-effective solutions will rely on automatic identification of suspicious regions by computer-aided diagnosis systems [1, 5].

In this work, the candidate lesion regions in given retinal images are treated as 'salient' and determined by using a low-rank analysis-based method [6]. *Saliency* usually means that an area stands out relative to its neighbors for its uniqueness or rarity features [7, 8]. In the field of

medical image analysis, saliency can describe suspected regions that contain indicative signs for diagnostic purposes, and will always command the attention of human experts [9]. Low-rank analysis has shown great potential for the detection of saliency [6, 10, 11]. Those parts with redundant information of an image usually show high regularities and lie in a low dimensional feature subspace. This can be approximated as a low-rank feature matrix. The salient part can be viewed as a sparse matrix [6]. To form the matrix for the low-rank analysis, a novel UNICOM feature is proposed, which seamlessly integrate UNIqueness and COMpactness features) for the representation of superpixels in images. The proposed framework for retinal lesion detection is a substantial extension to our previous work published in MICCAI-2018 [12] where only a uniqueness-based feature was proposed. In this work, the previous uniqueness-based feature is combined with a new compactness-based feature to form an integrated UNICOM feature, as the key input to the feature matrix of the given image for the subsequent low rank based saliency analysis. In essence, the uniqueness-based feature evaluates the rarity of image components whilst the compactness-based feature is a complementary feature to intensity for saliency description, to reduce the number of falsely-detected salient regions. Figure 2 illustrates the performance of the proposed framework on detecting salient regions of a retinal image. In identifying high-level contextual features and seeking to emulate human cognitive processes, the proposed method extracts EX, MA and HE at pixel level in retinal color fundus images, and LK in FA. In line with [13], MA and HE are called dark lesions and EX and LK as bright lesions during evaluating our work.

The main contributions of this paper can be summarized as follows. **(i)** We have proposed a novel adaption of the concepts of saliency and low-rank analysis to the field of retinal image analysis. **(ii)** A novel UNICOM feature is extracted for the representation of an image and form a matrix for low-rank analysis. **(iii)** The proposed method has undergone rigorous quantitative evaluation using seven publicly-available datasets including CF and FA images with four different types of retinal abnormalities. The results show that our method is more accurate and robust to variations in the location, size, intensity, inhomogeneity and modality of the data than the selected state-of-the-art ones for lesion detection.

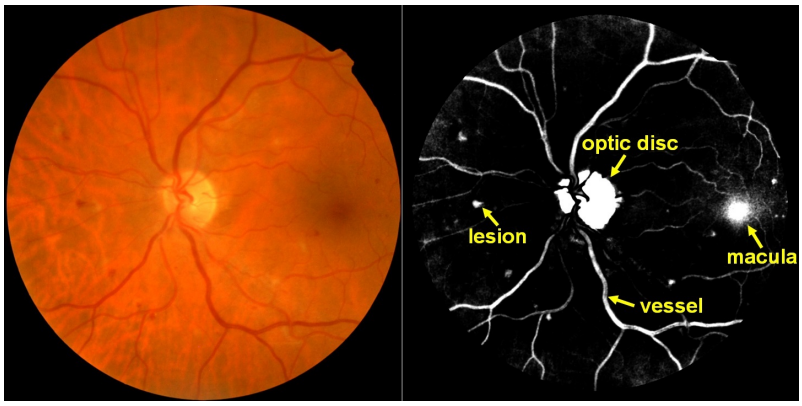

Figure 2: Examples of the proposed method on highlighting regions of interest (lesions, optic disc, vessel and the fovea) from an example retinal image.

2 Related Works

In recent years, developing health informatics systems for computer aided screening and grading of retinal diseases has received increasing attention, as evidenced by extensive reviews [5, 14], and the Diabetic Retinopathy: Segmentation and Grading Challenge at IEEE International Symposium on Biomedical Imaging (ISBI-2018)[1].

Existing methods rely on identifying suspected lesions from the analysis of fundus images, and they can be categorized into three groups based on their ability to detect different types of lesion: **i)** dark lesions such as MA and HE, **ii)** bright lesions such as EX and LK, and **iii)** combined dark and bright lesions.

Dark lesion detection. Fleming et al. [15] proposed an automated MA detection method using local contrast normalization and local vessel detection. A hybrid approach consisting of mathematical morphology and k-Nearest Neighbors (kNN) classification was introduced by Niemeijer et al. [1] for the MA extraction. Giancardo et al. [16] utilized a thresholding technique followed by a Radon transformation and support vector machine (SVM) for MA detection. Tang et al. [17] presented a splat feature classification method to detect retinal HE. This classification can model shapes of various lesions efficiently regardless of their variability in appearance, texture or size. A multi-agent system was proposed in [18] which uses gradient patterns and Gaussian fitting parameters in different directions to segment MA. Dai et al. [19] employed gradient vector analysis and

[1] `https://idrid.grand-challenge.org/Home/`

a class-imbalance classifier to determine MA candidates. Seoud et al. [3] generated a new set of shape features called Dynamic Shape Features to detect dark lesions from retinal images. Dashtbozorg et al. [4] used a gradient weighting-based iterative thresholding approach and a boosting classifier to locate MA.

Bright lesion detection. Phillips et al. [20] calculated the gradient of intensity, and then thresholded the gradient values to determine LK regions in DR images. In [21], the EX contours were determined by means of morphological reconstruction techniques. Sanchez et al. [22, 23] used a statistical technique called mixture model and contextual information to detect the EX. Welfer et al. [24] employed a coarse-to-fine strategy for detecting EX in retinal images. In [25], a set of features based on color, wavelet decomposition and automatic lesion segmentation were employed to train a classifier, which is able to detect EX in color fundus images. Agurto et al. [26] proposed an EX detection method based on optimal thresholding of instantaneous amplitude, and a partial least squares-based classification. Rabbani et al.[27] employed an active contour segmentation model to detect the boundaries of LK in FA images of subjects with diabetic macular edema. Zhao et al. [28] used the intensity and compactness features to generate a saliency map, and segment the precise LK area by using a graph-cut model. Liu et al. [29] presented a location-to-segmentation strategy for automatic EX segmentation in color retinal fundus images.

Combined bright and dark lesion detection. A visual word dictionary-based feature detection and analysis framework was proposed by Rocha et al. [30], which is capable of identifying MA and EX. Roychowdhury et al. [13] designed a system called DREAM for the grading of DR using machine learning. Non-lesions, or false positives, are rejected by the hierarchical classification, and the lesions are classified into bright and dark ones by using multiple classification criteria. Zhang et al. [31] proposed a multi-scale correlation coefficients-based method and a dynamic thresholding technique for retinal lesion extraction. A rule-based classification and dictionary learning algorithm was then employed for more accurate detection of retinal lesions. Gondal et al. [32] proposed to use a modified Convolutional Neural Network (CNN) in weak supervision with only image-level labels to identify lesions. Quellec et al. [33] generated a heat map as a key input for their deep learning approach - ConvNets. This network can be utilized for DR screening, and both bright and dark lesions are detected at the image level and at the lesion level respectively. However, as a deep learning technique this method is data hungry and limited by the data availability.

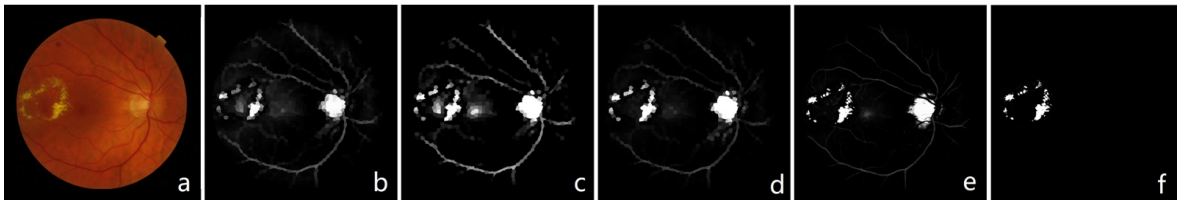

Figure 3: The main steps of the proposed method. (a) An example color fundus image; (b) Estimated uniqueness-based feature; (c) Estimated compactness-based feature; (d) Low-rank based saliency detection by using the combined uniqueness and compactness features; (e) Estimated saliency map at pixel-level; (f) Final lesion detection result after removing blood vessels, optic disc and macular regions.

The majority of previous approaches to lesion detection are based solely on morphological segmentation or classification [15, 16, 17, 19, 21, 13, 33, 32]. These strategies usually work on a single type of lesions with careful parameter optimization and training data collection, but often fail to work for the detection of other types of lesions without problem-specific optimization or information. It is therefore essential to develop generic algorithms with accurate and reliable performance for the detection of different types of lesions without over-relying on the need of handcrafted parameters or knowledge.

3 Proposed method

In this section, we detail our novel UNICOM feature based saliency detection model for retinal lesion detection. The main steps of our approach are illustrated in Figure 3. The details of these steps are described in these four subsections.

3.1 UNICOM saliency feature

Finding a good discriminative feature plays a key role in ensuring the validity of the saliency detection model. In this work, we propose a novel feature: the UNICOM, which combines intensity uniqueness and spatial compactness characteristics.

Perazzi et al. [34] suggest that the *uniqueness* of a component may reveal the rarity of an image component. Relative intensity is a commonly used property in the investigation of saliency [34]: salient regions stand out from their surroundings in certain aspects. Cheng et al. [35] suggest that

compactness can measure elemental distribution. These elements are more salient when they are grouped in a particular image region rather than evenly distributed over the whole image.

Inspired by the fact that human vision is usually more concerned with objects than with individual pixels and the objects of interest may vary in size, in this paper an input image is firstly partitioned into N superpixels $\{P_i\}_{i=1}^{N}$, by using the Simple Linear Iterative Clustering (SLIC) method [36]. Without loss of generality, we assume that N superpixels are generated, the colors of any two superpixels i and j, $1 \leq i, j \leq N$, are $\mathbf{c}_i$ and $\mathbf{c}_j$, while their positions are $\mathbf{p}_i$ and $\mathbf{p}_j$. The UNICOM feature U_i of superpixel i is then defined by combining the uniqueness of intensity $\mathcal{I}$ and the compactness of spatial distribution $\mathcal{D}$:

$$\mathbf{U}_i = \mathcal{I}_i \cdot \exp(-k \cdot \mathcal{D}_i), \tag{1}$$

where an exponential function is employed to emphasize $\mathcal{D}_i$, which is of higher significance and greater diagnostic capability than the intensity measurement $\mathcal{I}_i$ [34]. The parameter k represents the strength of the spatial weighting, and is set as 6 and -6 for dark and bright lesion detection, respectively.

3.1.1 Uniqueness feature generation

The uniqueness in the intensity domain I_i of superpixel i is estimated by computing the rarity compared to all the other superpixels j:

$$\mathcal{I}_i = \sum_{j=1, j\neq i}^{N} \|\mathbf{c}_i - \mathbf{c}_j\|^2 \cdot w^I(\mathbf{p}_i, \mathbf{p}_j). \tag{2}$$

where **c** indicates the intensity value. The local weighting function $w^I(\mathbf{p}_i, \mathbf{p}_j)$ is introduced here so that global and local contrast can be effectively combined with control over the influence radius. A standard Gaussian function is utilized to model the local contrast in terms of geometric distances between superpixels i and j:

$$w^I(\mathbf{p}_i, \mathbf{p}_j) = \frac{1}{\mathbf{Z}_i^I} \exp\{-\frac{\|\mathbf{p}_i - \mathbf{p}_j\|^2}{2\sigma_p^2}\}, \tag{3}$$

where standard deviation $\sigma_{\mathbf{p}}$ controls the range of the uniqueness operator from 0 to 1 (where 1 = global uniqueness) and was empirically set to 0.8. The normalization term $\mathbf{Z}_i^I$ ensures that $\sum_{j=1,j\neq i}^{N} w^I(\mathbf{p}_i, \mathbf{p}_j) = 1$. Eqn.2 can be decomposed by factoring out:

$$\begin{aligned}\mathcal{I}_i = \mathbf{c}_i^2 \underbrace{\sum_{j=1,j\neq i}^{N} w^I(\mathbf{p}_i, \mathbf{p}_j)}_{1} \\ - 2\mathbf{c}_j \underbrace{\sum_{j=1,j\neq i}^{N} \mathbf{c}_j w^I(\mathbf{p}_i, \mathbf{p}_j)}_{\text{Gaussian blur } \mathbf{c}_j} + \underbrace{\sum_{j=1,j\neq i}^{N} \mathbf{c}_j^2 w^I(\mathbf{p}_i, \mathbf{p}_j)}_{\text{Gaussian blur } \mathbf{c}_j^2}.\end{aligned} \tag{4}$$

It can be seen from Eqn.4 that both terms $\sum_{j=1,j\neq i}^{N} \mathbf{c}_j w^I(\mathbf{p}_i, \mathbf{p}_j)$ and $\sum_{j=1,j\neq i}^{N} \mathbf{c}_j^2 w^I(\mathbf{p}_i, \mathbf{p}_j)$ can be regarded as the Gaussian blurring kernel on intensities $\mathbf{c}_j$ and their squares $\mathbf{c}_j^2$, respectively. Figure 3 (b) depicts an example of the proposed uniqueness-based feature.

3.1.2 Compactness feature generation

Cheng et al.[35] suggest that spatial variance is a potential measure of an element's distribution. Low variance of its compactness implies that an element should be considered more salient than one that is spatially more widely distributed. The human visual system tends to pay more attention to a more compact object than to a more diffuse object [6, 28]. The measure of compactness of an object might therefore be of use as a complementary feature to intensity for saliency analysis. Similarly, the compactness of spatial distribution $\mathcal{D}_i$ is estimated as:

$$\mathcal{D}_i = \sum_{j=1,j\neq i}^{N} \|\mathbf{p}_j - \mu_i\|^2 \cdot w^D(\mathbf{c}_i, \mathbf{c}_j), \tag{5}$$

where $\mu_i = \sum_{j=1,j\neq i}^{N} \mathbf{p}_j w^D(\mathbf{c}_i, \mathbf{c}_j)$ defines the weighted mean position of positions $\mathbf{p}_j$, and $w^D(\mathbf{c}_i, \mathbf{c}_j)$ indicates the degree of similarity between colors $\mathbf{c}_i$ and $\mathbf{c}_j$. As in Eqn.2, the color similarity weight is also estimated using a Gaussian function $w^D(\mathbf{c}_i, \mathbf{c}_j) = \frac{1}{\mathbf{Z}_i^D} \exp\{-\frac{\|\mathbf{c}_i - \mathbf{c}_j\|^2}{2\sigma_c^2}\}$, where $\mathbf{Z}_i^D$ can be defined as to $\mathbf{Z}_i^I$, while σ_c controls the sensitivity of the spatial distribution: larger values of σ_c indicate increased values of spatial distribution, and vice versa. It was also empirically set to 0.8.

Eqn.5 can be expanded as:

$$\begin{aligned}\mathcal{D}_i &= \sum_{j=1,j\neq i}^{N} \mathbf{p}_j^2 w^D(\mathbf{c}_i,\mathbf{c}_j) \\ &- 2\mu_i \underbrace{\sum_{j=1,j\neq i}^{N} \mathbf{p}_j w^D(\mathbf{c}_i,\mathbf{c}_j)}_{\mu_i} + {\mu_i}^2 \underbrace{\sum_{j=1,j\neq i}^{N} w^D(\mathbf{c}_i,\mathbf{c}_j)}_{1} \\ &= \underbrace{\sum_{j=1,j\neq i}^{N} \mathbf{p}_j^2 w^D(\mathbf{c}_i,\mathbf{c}_j)}_{\text{Gaussian blur } \mathbf{p}_j^2} - \underbrace{\mu_i^2}_{\text{Gaussian blur } \mathbf{p}_j}.\end{aligned} \tag{6}$$

Again, both terms $\sum_{j=1,j\neq i}^{N} \mathbf{p}_j w^D(\mathbf{c}_i,\mathbf{c}_j)$ and μ_i^2 can be effectively treated as Gaussian blurring. It will be observed that the more distinct superpixel i is from superpixel j, the larger the value of $\mathcal{D}_i$, and vice versa. Figure 3 (c) shows an example of the proposed compactness-based feature.

By incorporating the compactness feature $\mathcal{D}_i$ with the uniqueness feature $\mathcal{I}_i$ of a given image, the UNICOM feature $\mathbf{U}_i$ is calculated using Eqn.1.

3.2 Saliency detection

Low-rank and sparsity analysis provides a useful tool for detecting salient regions [6]. A region with high regularities (redundancy or background) usually lies in a low dimensional feature subspace, which can be approximated as a low-rank feature matrix, while a salient region can be represented by a sparse feature matrix. The term *sparsity* shares some similarities with the perception of *contrast*, which implies that the pixels or regions differ significantly from their surroundings. The relation between sparsity and saliency follows the fact that only distinctive sensory information is selected for further processing in a human vision system.

D-dimension features are extracted from each superpixel including the above-obtained UNICOM feature, and the stacked feature vectors form a matrix representation of the input image as $\mathbf{F} = [f_1, f_2, \cdots, f_N] \in \mathbb{R}^{D\times N}$. In this work, 31 features were used to form the feature matrix, and the feature details and importance of these features will be listed and discussed in Sec. VI. C.

The saliency detection task may then be further modeled as a low-rank matrix recovery problem [37]:

$$\min_{\mathbf{L},\mathbf{S}} \mathit{rank}\,(\mathbf{L}) + \lambda\|\mathbf{S}\|_0 \quad \text{s.t.} \quad \mathbf{F} = \mathbf{L} + \mathbf{S}, \tag{7}$$

where $\|*\|_0$ denotes the l_0-norm, and $\mathbf{L}$ is the low-rank matrix corresponding to the background.

This suggests that matrix $\mathbf{L}$ may have the property of low-rankness. $\mathbf{S}$ is the sparse matrix representing the salient parts, and these usually display characteristic and spatial coherence. Since such a problem takes non-deterministic polynomial time[37], one can alternatively solve its convex surrogate instead for computational efficiency and feasibility:

$$\min_{\mathbf{L},\mathbf{S}} \|\mathbf{L}\|_* + \lambda\|\mathbf{S}\|_1 \quad \text{s.t.} \quad \mathbf{F} = \mathbf{L} + \mathbf{S}, \tag{8}$$

where $\| * \|_*$ and $\| * \|_1$ denote the nuclear norm and l_1-norm of $\mathbf{L}$ and $\mathbf{S}$, respectively. Various algorithms that can be used to estimate the sparse matrix $\mathbf{S}$, and the Robust Principal Component Analysis (Robust PCA) [38, 37] is a powerful tool to recover the decomposed low-rank $\mathbf{L}$ and sparse $\mathbf{S}$ matrices. We refer to [37] for more details on Robust PCA. The saliency map is generated by assembling the l_1-norm of each column S_i in $\mathbf{S}$ from the corresponding segments, and further normalized into grayscale for display and visualization.

In medical image analysis, uniformly sampled patches often display large feature variations, such as a high degree of anatomical variation across the population and the complexity of the surrounding tissue/organs, and these characteristics may affect the accuracy of saliency detection. On one hand, some generated patches may contain both background and salient regions, and this may lead to an invalid assumption that the background has a low-rank. On the other hand, if the salient region is large, it may be decomposed into many patches, and these fragmented patches will then not be salient because they are no longer identified as sparse.

Decomposing $\mathbf{F}$ in the original feature space usually produces inferior saliency detection results, as the sparse analysis only ensures that a single patch is encoded as a sparse vector, which may not correspond to the saliency over the entire image. The authors of [6] instead trained a linear transformation matrix $\mathbf{T}$ on the feature space from a set of training images:

$$\min_{\mathbf{L},\mathbf{S}} \|\mathbf{L}\|_* + \lambda\|\mathbf{S}\|_1 \quad \text{s.t.} \quad \mathbf{TF} = \mathbf{L} + \mathbf{S}. \tag{9}$$

In this new space, the variation of the background features was also considered, and their transformations are more likely to lie in a low dimensional sub-space and can thus be represented as a low-rank matrix. After transformation, the method is more sensitive to color changes in saliency detection. The reader should refer to [6] for more details on the determination of $\mathbf{T}$.

3.3 Saliency refinement

The saliency of each pixel is temporarily assigned the saliency value of the superpixel of which it is a member, in other words, the saliency values are taken at superpixel level, as shown in Figure 3 (d), and are obtained by determining $\mathbf{S}$ of Eqn.9. Further refinement is then required in order to assign the saliency value at pixel level by employing a bilateral filter [6], since it is more robust to imaging noise and the variation of imaging resolution and scale. That is, the saliency value $\mathbf{S}'_u$ of each image pixel u is estimated as the weighted average of the saliency values of other pixels v:

$$\mathbf{S}'_u = \sum_{v=1}^{T} w_{uv}\mathbf{S}_v, \tag{10}$$

where T is the total number of pixels in the image, $\mathbf{S}$ is the saliency map at superpixel level, and the Gaussian weight w_{uv} is defined as $w_{uv} = \frac{1}{\mathbf{Z}_u}\exp(-\frac{1}{2}(\alpha\|\mathbf{c}_u - \mathbf{c}_v\|^2 + \beta\|\mathbf{p}_u - \mathbf{p}_v\|^2))$, where $\mathbf{Z}_u$ is defined in similar manner to $\mathbf{Z}_i^D$ above. A weighted Gaussian filter which considers both color and position is applied to the saliency map $\mathbf{S}$ at superpixel level, in order to achieve the translation of per-superpixel saliency to per-pixel saliency. The trade-off between intensity and position is controlled by parameters α and β, both of which were set to 0.01 in the present work. The final saliency map highlights salient object regions of interest by suppressing the background of the image. Figure 3 (e) demonstrates the performance of this saliency refinement, and the property of human vision by which attention declines as the edge of the area of interest is approached may be mimicked.

3.4 Post-processing

The exact contours of the lesions can be finally extracted from the generated saliency map after removing confounding structures such as blood vessels, the optic disc, and the macular. The following steps are applied.

Blood vessel segmentation: We used the infinite perimeter active contour with hybrid region (IPACHR) method [39] to extract the retinal vasculature. IPACHR introduces a novel active contour model, and has the superior power in segmenting components with irregular and oscillatory boundaries [40]. In addition, IPACHR considers both vesselness map based on local phase and intensity of an image, so as to further improve the segmentation performance compared to the typical infinite perimeter active contour model.

Table 1: Details of the retinal image datasets employed, and the values of controlling parameter k for each dataset.

Datasets	No. Img.	Size	FOV	Lesions	Disease	Groundtruth	Para. k
RC-RGB-MA	250	2595×1944	45°	MA	DR	Lesion level	6
DiaretDB1	89	1500×1152	50°	MA, HA, EX	DR	Lesion level	6
ROC	100	$768 \times 756 - 1394 \times 1392$	45°	MA	DR	Lesion level	7
e-ophtha	195	$1440 \times 960 - 2544 \times 1696$	45°	MA, EX	DR	Pixel level	5
Messidor	1200	2304×1536	45°	MA, HA, EX	DR	Image level	-5
DME-DUKE	24	768×768	55°	LK	DR	Pixel level	-6
LIMA	30	$2189 \times 3061 - 3715 \times 2733$	50°	LK	MR	Pixel level	-6

Optic disc detection: Usually, it has been well observed that any region with several surrounding vessels greater than a threshold of 5 [41] will be assumed to be the optic disc, and will be removed. In our experiments this method is efficient and effective. However, other sophisticated optic disc detection methods [42, 43] may work equally well.

Macular detection: The macular region can be masked out by using the Gaussian Mixture Model (GMM) proposed by [44]. Note, the source codes with default parameter settings provided by the authors for these methods were used.

4 Datasets and Evaluation Metrics

To evaluate its effectiveness, we have evaluated the proposed method on seven publicly-available retinal image datasets showing diabetic or malarial pathogenesis. These were: the Retina Check project managed by Eindhoven University of Technology (RC-RGB-MA) [4]; the DiaretDB1 [45]; the Retinopathy Online Challenge training set (ROC) [46]; the e-ophtha [47]; the Messidor [48]; the Diabetic Macular Edema (DME-DUKE) [27] dataset collected by Duke University; and the Malarial Retinopathy dataset collected by the University of Liverpool (LIMA) [41]. Table 1 summarizes the key information of these datasets. To achieve a single set of parameters, all the images from different datasets were uniformly down-sampled to 768×768. Note, the ground truth type of lesion level indicates that the manual annotation was made by using a single pixel (center of the lesions) or a coarse boundary (a disc could cover the entire lesion region); Image level shows that the ground truth is graded as presence or absence of lesions; Pixel level reveals that the ground truth is marked by labeling a precise contour of the lesion regions. The first five datasets are retinal color fundus image, while the rest are fluorescein angiogram.

Two experts used an annotation tool to locate candidate MAs in RC-RGB-MA, and their consensus was used for evaluation. Four experts annotated the MAs, HAs, and EXs independently for DiaretDB1 by drawing a disc over the lesions, and reported confidence levels $\{< 50\%, \geq 50\%, 100\%\}$. The consensus of agreement higher than 75% was used to assign a region as a lesion. For the ROC dataset, four experts indicated the center location of the MAs, and the logical OR was used to combine the lesion locations and mark them as MAs. The MAs and EXs in e-ophtha were manually annotated by an ophthalmologist who marked the lesion contours: a second ophthalmologist checked these annotations. The Messidor dataset was annotated regarding two significant criteria: retinopathy grade, and risk of macular edema. For more details of grade criteria, we refer the readers to [5]. The leakage contours of the DME-DUKE dataset were manually annotated by two independent graders and later reviewed for intra-observer reliability. For the LIMA dataset, one grader defined the boundaries of each large focal leak, and a second grader checked these annotations.

The evaluations of these datasets were undertaken in three different ways, based on the types of available manual annotations. A lesion-based approach defined candidate lesions and counted them; a pixel-based approach focused on the location of lesions; and the image-based approach aimed simply to determine whether a lesion was present.

To compare the detection results of the proposed method with their corresponding manual annotations by human graders, the following metrics were employed: *sensitivity (SE)* $= TP/(TP + FN)$, *specificity (SP)* $= TN/(TN + FP)$, and the area under the ROC curve (AUC), where TP, TN, FP and FN indicate true positive (correctly identified lesion pixels or regions), true negative (correctly identified background pixels or regions), false positive (incorrectly identified lesion pixels or regions), and false negative (incorrectly identified background pixels or regions), respectively.

5 Experimental Results

Once the saliency map has been generated, a threshold value T = 0.65 (which achieved the highest AUC scores) was applied to the saliency map to obtain the candidate lesion regions for all the datasets. Large blood vessels, the macular and the optic disc may also be enhanced as candidate lesion regions or region of interest (ROI), as these regions are conspicuous objects in retinal images,

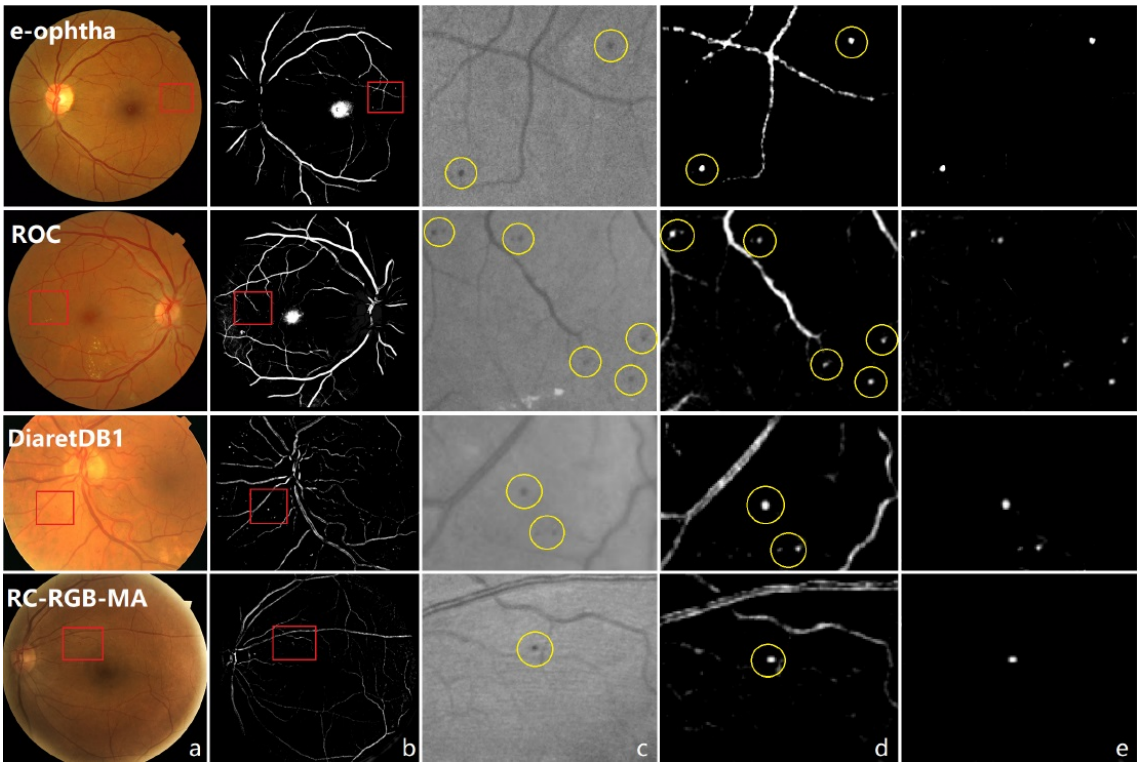

Figure 4: **Microaneurysm** detection results of the proposed method over four example images, one from each of four datasets. (a) Example images; (b) Saliency maps of (a); (c) Zoom-in view of the selected regions, and yellow circles indicate the locations of MAs; (d) Zoom-in view of saliency maps of the selected regions; (e) Detected MAs.

and can easily be distinguished visually by their intensity or shape, as shown in Figures 4-7. True retinal lesions can be identified by simply masking away the blood vessels and the optic disc from the produced saliency map. Figure 3 (f) shows the extracted lesion regions.

In these subsections, the performance of the proposed method is rigorously validated for the detection of dark lesions and bright lesions.

5.1 Dark lesion detection

A large number of studies, i.e., ([3, 31, 25]) have performed lesion detection on prevalence of referable at image level, but it is difficult to understand the criteria for selecting true positives and false negatives. In the study of MA detection, the sensitivity values against the average number of false positives per image (FPI) was used to measure performance [46]. It was obtained by averaging

Table 2: **Microaneurysms** detection result: Sensitivities of different methods at the predefined rates of false positives per image over four different datasets.

Dataset	Method	1/8	1/4	1/2	1	2	4	8	FS
e-ophtha	Dashtbozorg et al. [4]	0.358	0.417	0.471	0.522	0.558	0.605	0.638	0.510
	Wu et al. [50]	0.063	0.117	0.172	0.245	0.323	0.417	0.573	0.273
	Zhang et al. [31]	0.170	0.240	0.320	0.440	0.540	0.630	0.740	0.440
	Proposed	0.325	0.387	0.443	0.501	0.551	0.637	0.738	**0.512**
ROC	Dashtbozorg et al. [4]	0.435	0.443	0.454	0.476	0.481	0.495	0.506	0.471
	Wang et al. [51]	0.273	0.379	0.398	0.481	0.545	0.576	0.598	0.464
	Wu et al.[50]	0.037	0.056	0.103	0.206	0.295	0.339	0.376	0.202
	Dai et al. [19]	0.219	0.257	0.338	0.429	0.528	0.598	0.662	0.433
	Proposed	0.254	0.335	0.388	0.420	0.540	0.630	0.725	**0.472**
DiaretDB1	Dashtbozorg et al. [4]	0.507	0.517	0.519	0.542	0.555	0.574	0.617	**0.547**
	Seoud et al. [3]	0.140	0.175	0.250	0.323	0.440	0.546	0.642	0.359
	Dai et al. [19]	0.035	0.058	0.112	0.254	0.427	0.607	0.755	0.321
	DRSCREEN [49]	0.001	0.003	0.009	0.020	0.059	0.140	0.257	0.070
	Proposed	0.163	0.201	0.279	0.365	0.501	0.612	0.723	0.406
RC-RGB-MA	Dashtbozorg et al. [4]	0.541	0.591	0.618	0.662	0.697	0.704	0.714	0.647
	Proposed	0.512	0.588	0.621	0.673	0.704	0.735	0.741	**0.653**

the sensitivities taken at 7 points along the free-response receiver operating characteristic curve. Sensitivity values for FPI rates of 1/8, 1/4, 1/2, 1, 2, 4, and 8 were thus obtained. A final score (FS) was computed by averaging the sensitivity values obtained at these seven predefined FPIs [49]. The sensitivity indicates the proportion of MAs correctly detected, and the FPI represents the number of non-MAs incorrectly detected as MAs. Figures 4 (b) and (d) show that the proposed method successfully detected the MA regions as salient. The exact MA regions could then be located after removing other ROIs. Table 2 compares the MA detection performances of different methods in terms of sensitivity against FPI on the e-ophtha, ROC, DiaretDB1, and recent released RC-RGB-MA datasets respectively. For brevity, we provide readers with the performance only from the three most recent MA detection methods (note, only [4] reports the detection performance on the RC-RGB-MA dataset): this is not intended to be taken as exhaustive. As observed, the proposed method outperforms the existing state-of-the-art ones on all the four datasets in terms of final score.

Figure 5 demonstrates the ability our method to detect HE on two randomly selected images from DiaretDB1 and Messidor datasets. In contrast to the MA detection, the HE detection has received relatively little attention [33, 32, 52], and in the literature performance has been evaluated only on DiaretDB1. Table 3 reports the sensitivity values achieved by different methods on the DiaretDB1 dataset. Evaluation was undertaken at image and pixel level respectively. It can be seen that the proposed method achieves the best performance at both the image and lesion levels with the highest sensitivity values of 0.981 and 0.790 respectively. While both the deep-learning based

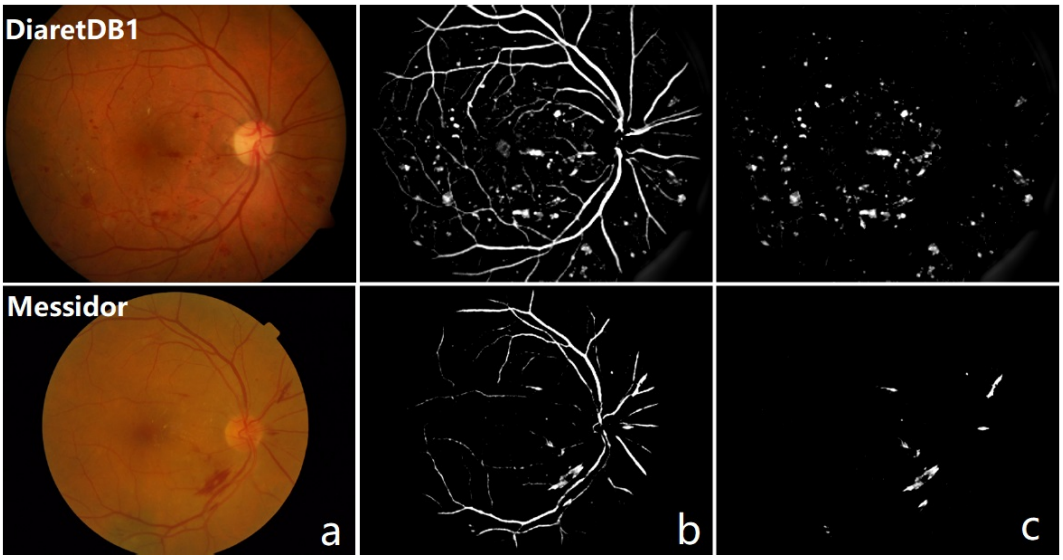

Figure 5: The **hemorrhage** detection results of the proposed method on two example images from the DiaretDB1 and Messidor dataset. (a) Original images; (b) Generated saliency map; (c) Detected hemorrhage regions.

Table 3: Sensitivity scores of different methods for the detection of **Hemorrhages** at image level and pixel level over the **DiaretDB1** dataset respectively. Note, the methods compared only reported their performances on sensitivity.

	Image level	pixel level
Quellec et al. [33]	0.947	0.710
Gondal et al. [32]	0.972	0.720
Zhou et al. [52]	0.944	-
proposed	0.981	0.790

approaches [33, 32] focus on the detection of class-specific discriminative regions, the downsampling operator in their architecture results in loss of location information, and the upsampling operator tends to produce a coarse feature map that renders the fine grained lesion localization impossible.

Different types of dark lesions (MA and HE) may appear in a single retinal image. Therefore, a comparative analysis of different methods in their detection is shown in Table 4. It can be observed that the proposed method has a favorable detection performance compared to the existing ones. To be more specific, the proposed method has produced a sensitivity value of 0.978, specificity of 0.955, and AUC of 0.964 on the DiaretDB1 dataset (at image level). It may be observed that our SE score of dark lesion detection is lower than HE only detection in Table 3. This phenomenon suggests that the combination of multiple lesions is more challenging to detect.

Table 4: The SE, SP, and AUC values of different methods for dark lesion (hybrid of MA and HE) detection at image level over the **DiaretDB1** dataset.

	SE	SP	AUC
Kauppi et al. [45]	0.972	0.720	-
Roychowdhury et al. [13]	0.800	0.850	0.834
Rocha et al. [30]	0.900	0.830	0.933
Quellec et al. [33]	-	-	0.963
Proposed	0.978	0.955	0.964

Table 5: The SE, SP, and AUC values of different methods for the detection of **Exudates** over three different datasets.

Dataset	**Method**	SE	SP	AUC
DiaretDB1	Zhang et al. [31]	-	-	0.950
	Giancardo et al. [25]	0.860	0.850	0.953
	Quellec et al. [33]	0.809	-	-
	Walter et al. [32]	0.660	0.986	-
	Welfer et al. [21]	0.705	0.988	-
	Roychowdhury et al. [13]	0.742	0.980	-
	Liu et al. [29]	0.830	-	-
	Haloi et al. [53]	0.965	-	-
	Rocha et al. [30]	0.700	0.990	0.881
	Proposed	0.891	0.980	0.964
Messidor	Agurto et al. [26]	1.000	0.730	-
	Giancardo et al. [25]	-	-	0.900
	Zhang et al. [31]	-	-	0.930
	Rocha et al. [30]	0.900	0.640	0.893
	Proposed	0.912	0.950	0.941
e-ophtha	Decencire et al. [47]	0.809	0.815	-
	Giancardo et al. [25]	-	-	0.870
	Zhang et al. [31]	0.830	-	-
	Proposed	0.856	0.910	0.895

* The evaluations were undertaken at lesion level for DiaretDB1, image level for Messidor, and pixel level for e-ophtha.

5.2 Bright lesion detection

The presence of exudates has been used to grade the risk of macular edema. Therefore, it is important to detect and validate the presence of exudate. We evaluate the exudate detection performance through the DiaretDB1, e-ophtha, and Messidor datasets. Both the DiaretDB1 and e-ophtha datasets provide a lesion map generated by experts. While the Messidor dataset does not manually annotate exudate contours, it provides a DR severity grading and contains information on the risk of macular edema for each image.

Figure 6 depicts the saliency and exudate detection results of the proposed method over the images from Messidor, DiaretDB1 and e-ophtha respectively. Table 5 shows the SE, SP and AUC values of different methods. The proposed method achieves higher sensitivity, specificity, and AUC values over DiaretDB1, e-ophtha, and Messidor when compared with the existing ones. It produced the highest AUC scores of 0.952, 0.950, and 0.941, respectively. Our method exhibits superior

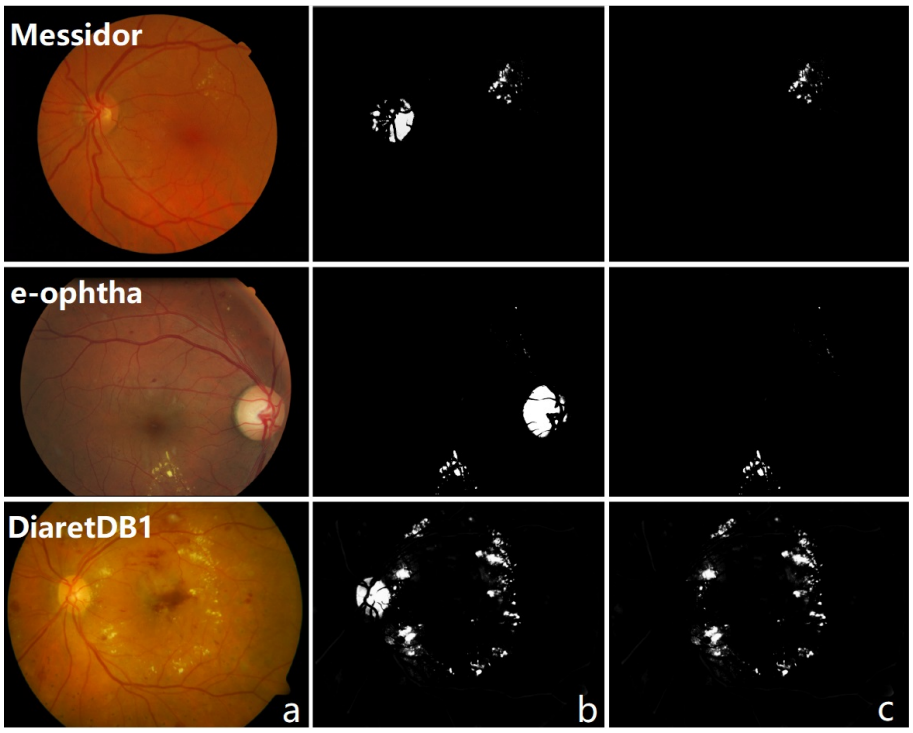

Figure 6: The detection results of **Exudate** using the proposed method in three example images, one from each of the three different datasets: (a) Example images; (b) Detected saliency; (c) Detected exudate regions.

performance on DiaretDB1. For example, the sensitivity score of the method by Roychowdhury et al. [13] would drop to 0.742 in order to achieve the same specificity score of 0.980. Even though the sensitivity score of Agurto's method reaches 1.000, its specificity score is only 0.730, which is much lower than 0.950 by our method. It is worth noting that the AUC scores obtained by Zhang [31] were computed at image level (presence of exudate).

In contrast to the large number of studies on detecting various lesions (MA, HE, and EX), relatively few methods have been proposed for automated detection of leakage. Leakage in angiography is an important sign for clinicians to determine the relative activity and progression of the underlying disease. In this work, performing the proposed method on leakage detection was obtained over two FA image datasets: DME-DUKE with DR pathology, and LIMA with MR pathology: Figure 7 shows one example from each. Table 6 shows the performances of different methods in detecting leakage sites in terms of sensitivity, specificity, and AUC at pixel level. It can be observed that the performances of our proposed method are again significantly better than

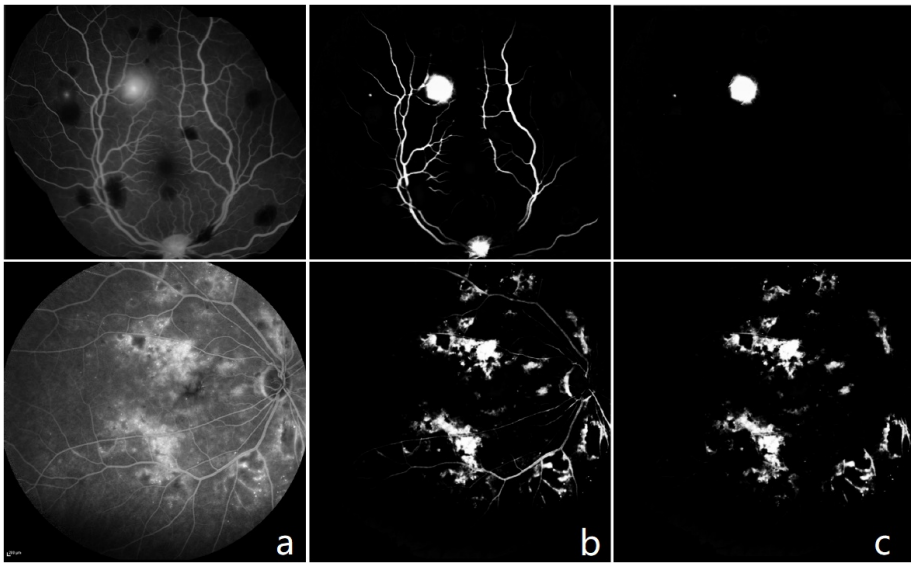

Figure 7: **Leakage** detection results of the proposed method on two example images from the LIMA and DUKE-DME datasets respectively. (a) Original images; (b) The generated saliency map; (c) Detected leakage regions.

Table 6: The SE, SP and AUC scores of different methods for the detection of **Leakage** over two different datasets.

Dataset	**Method**	SE	SP	AUC
DUKE-DME	Rabbani et al. [27]	0.690	0.910	0.800
	Zhao et al. [28]	0.780	0.940	0.860
	proposed	0.810	0.930	0.870
LIMA	Rabbani et al. [27]	0.810	0.870	0.840
	Zhao et al. [28]	0.930	0.960	0.940
	Proposed	0.950	0.950	0.950

those compared ones.

6 Discussion and Conclusion

The extensive validation of the proposed retinal lesion detection method on seven publicly accessible datasets with different pathologies and imaging modalities demonstrates its high potential to be a powerful tool in the analysis of a wide spectrum of eye diseases. In this section, the method is further investigated in terms of saliency analysis, saliency cues and feature importance.

6.1 Comparison to the state-of-the-art saliency detection methods

In the past decade, many saliency detection methods have been proposed. To decide which of the saliency detection methods is superior when applied to retinal images, a comparison was made between five state-of-the-art saliency detection methods regarding candidate lesion detection: the classic saliency detection method proposed by Itti et al. [7], spectral residual saliency [54], frequency-tuned saliency [55], graph-based visual saliency [56] and context-aware saliency [57]. The competitors are referred to here as IT, SR, FT, GB, and CA, respectively. The source codes, with default parameter settings provided by the authors, were used for all these methods.

Figure 8 depicts saliency detection results by six methods over two images. The proposed method identifies more comprehensive areas of saliency, which is consistent with the results obtained by human visual inspection - both dark and bright lesions are highlighted as salient. The SR method has the poorest performance, since spatial information is absent in the Fourier representation, where the Fourier domain spectral energies derived from frequency bands alone are not sufficient. The proposed model is not only capable of suppressing background, but also highlights all salient regions (e.g., lesions, vessels, and the optic disc) with well-defined boundaries. By utilizing the UNICOM feature, the proposed method can better handle the issues of heterogeneous objects, poor contrast between object and background, large-scale and small-scale salient objects more effectively compared with other saliency detection ones.

To evaluate the saliency detection performance objectively, the FPR and TPR of the saliency maps derived by different methods were calculated. The ROC curves were obtained by varying the threshold value in increments of 0.01 in [0, 1], and observing the variation in SE versus (1-SP) each time. The evaluations were undertaken for the detection of dark and bright lesions separately across the aforementioned seven datasets. The averaged results of our method and its competitors are plotted in Figure 9 (a). It can be seen that our method achieves the best performance for both dark and bright lesion detection.

6.2 Effectiveness of each saliency cue

To validate the effectiveness of saliency cues in the proposed low-rank-based saliency analysis method, we generated three receiver operating characteristics curves of the proposed method tak-

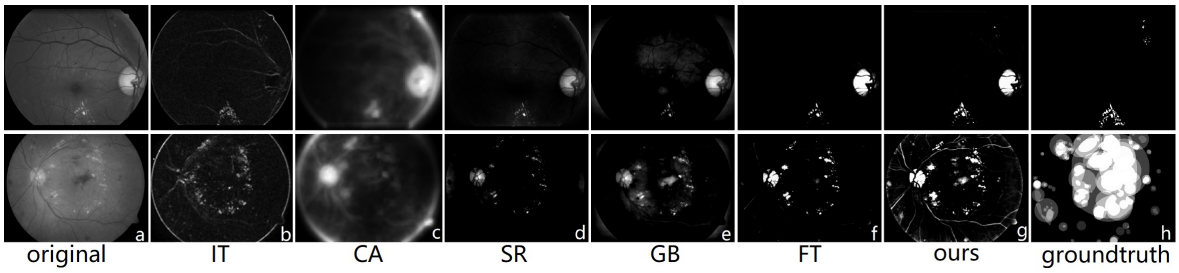

Figure 8: Saliency detection results of different algorithms over two example retinal images. (a) Original images. (b)-(g) Saliency maps generated using different methods. (h) Ground truth at lesion level: coarse lesion regions are annotated.

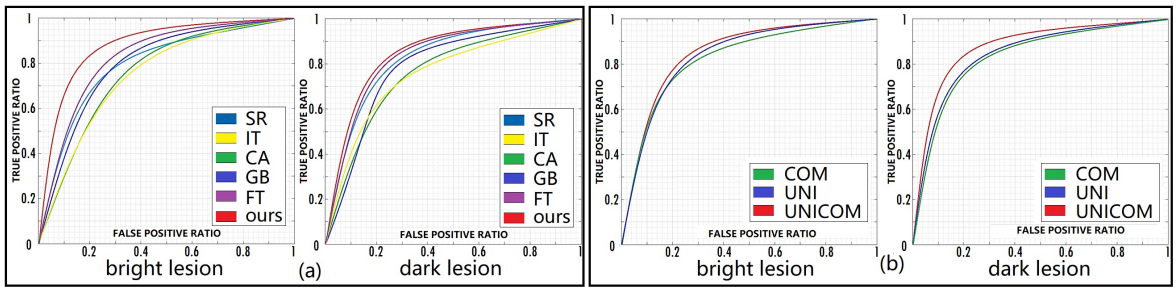

Figure 9: (a) Receiver operating characteristics curves of different saliency analysis methods for the detection of bright and dark lesions; (b) Receiver operating characteristics curves of the proposed method with different feature cues for the detection of bright and dark lesions respectively.

ing different cues: uniqueness cue only; compactness cue only; and combined uniqueness and compactness cues (UNICOM).

The ROC curves in Figure 9 (b) show that the UNICOM feature performs better than either the uniqueness or compactness feature alone. The proposed method combines uniqueness of intensity and spatial distribution with the compactness of the image component, as a global constraint on the saliency representation: the lesion regions have particular color (intensity) and shape (spatial) characteristics. The uniqueness cue evaluates how different each respective element is from all the other ones in an image, essentially measuring the relative 'rarity' of each element. The uniqueness cue is also able to detect high similarity between multiple regions in the image and to suppress globally repeated features. The compactness cue renders unique elements more salient when they are grouped in a particular image region, rather than evenly distributed over the whole image. The compactness cue is effective in distinguishing a salient region against background. The UNICOM

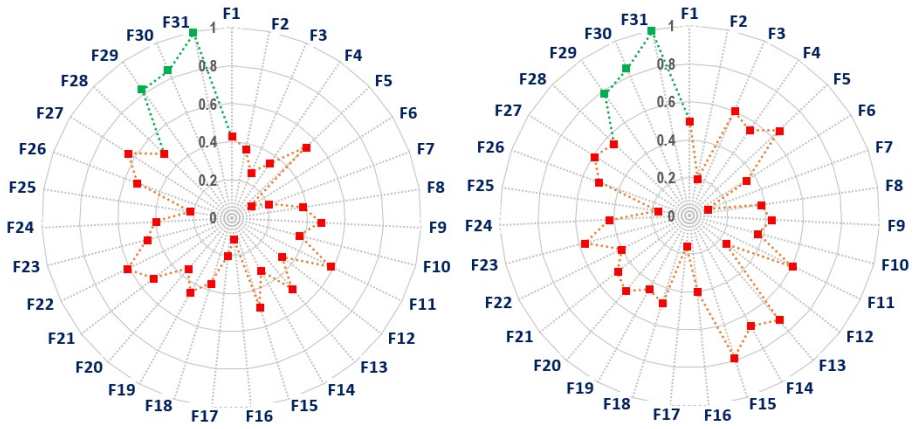

Figure 10: The relative importance of different features in the proposed method for the detection of different lesions. Left: bright lesion. Right: dark lesion.

Table 7: List of feature vectors for classification.

Feature notations	Descriptions
F_{1-5}	Max, min, mean, standard deviation, and entropy on intensity values of candidate patch in gray level.
F_{6-20}	Max, min, mean, standard deviation, and entropy on intensity values of candidate patch in R, G, B channels.
F_{21-23}	The color histogram of RGB, hue and saturation.
F_{24-28}	Max, min, mean, standard deviation, and entropy of the coordinates of centroid of candidate patch.
F_{29-31}	The proposed uniqueness-based, compactness-based and UNICOM feature.

feature combines the complementarity of uniqueness and compactness measures for a more powerful representation of saliency.

6.3 Feature importance analysis

In this section, the importance of the extracted features is investigated, to show the relative contribution of different features to saliency analysis and lesion detection. Totally a set of 31 features were stacked vertically to form a feature vector, as shown in Table 7. We measured the AUC scores 31 times for each dataset, omitting each factor in turn from the stacked feature vector for saliency detection via the low-rank matrix recovery. The importance score was estimated as $IS = 1 - SF_n$, where SF_n indicates the AUC score when feature F_n was excluded from the stacked feature vector for saliency analysis and lesion detection. The importance scores were then normalized into [0, 1], where 1 indicates that the feature has the greatest effect on lesion detection, and 0 shows that the feature does not effect on detection performance. Again, the analysis was

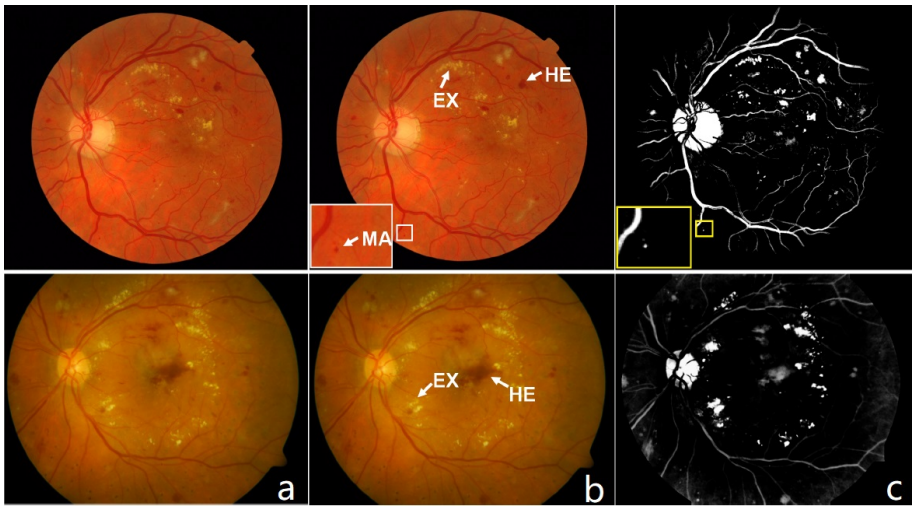

Figure 11: The detection results of different types of lesion regions by the proposed method: (a) Original images; (b) Manually annotated lesions; (c) Detected regions of interest.

undertaken over two separate tasks: detection of bright and dark lesions. The obtained feature importance maps are shown in Figure 10. As expected, the results demonstrate that the uniqueness-based, compactness-based and UNICOM features are the most important descriptors among these 31 features, as illustrated in green in Figure 10.

6.4 Conclusions

Developing the proposed method was motivated by medical demands for effective tools to quantify different types of lesions in retinal images. The accurate detection of retinal lesions is a challenging problem due to variations across patients, image intensity inhomogeneity, irregular shape and appearance of lesions., a novel low-rank-based saliency detection method was proposed to address this challenge, based on the novel UNICOM feature derived from the global intensity and spatial distribution of superpixels of the image.

Our extensive literature review shows that a single reliable method for automated detection of multiple lesions at pixel level is relatively unexplored. To the best of our knowledge, this is the first study on a new technique that is capable of the automated detection of hemorrhages, microaneurysms, exudates, and leakage from both CF and FA images. The experimental results, based on seven publicly-accessible DR and MR datasets, show that our method outperforms the

most recent alternative methods. The proposed method is not only capable of identifying the presence of lesions in an image, but also can accurately locate and measure the size of such lesions.

It is interesting to note that the evaluation metrics demonstrate that our method has better performances than the recent attention attracting deep learning-based approaches [33, 32]. It is believed that while the latter focuses on the detection of class-specific features and high classification accuracy, its architecture essential downsampling and upsampling operators imply that it has inherent difficulty in determining the exact location of the features in the original images and thus poor performance in detecting lesion regions at pixel level.

As shown in Figure 11, our saliency-driven method can detect both dark and bright lesions with no complicated parameter tuning or training data collection. These lesions may be distinguished by measuring the object size (which separates the MA from the HE), or intensity value (which discriminates between the dark and bright lesions). As may be observed from Figure 11, the proposed method is able to detect the vasculature, optic disc, macular, and abnormalities as salient regions. It is therefore possible that in future work our method might be adapted for other challenging tasks such as retinal vessel segmentation, optic disc detection and macular extraction. Therefore, with the superior performance that we have demonstrated in this paper, it is our belief that the proposed method will be a significant contribution to health informatics and will provide a powerful tool for retinal image analysis and beyond with great potential for improved healthcare and patient benefit.

7 Acknowledgment

This work was supported by National Science Foundation Program of China (61601029), Zhejiang Provincial Natural Science Foundation (LZ19F010001), Ningbo Natural Science Foundation (2018A610055), Grant of Ningbo 3315 Innovation Team.

References

[1] Niemeijer M., Abràmoff M. D., Ginneken B.. Image structure clustering for image quality verification of color retina images in diabetic retinopathy screening *Med. image anal.*. 2006;10:888–898.

[2] MacCormick I., Beare N., Taylor T., et al. Cerebral malaria in children: using the retina to study the brain *Brain.* 2014:2119-2142.

[3] Seoud L., Hurtut T., Cheriet F., Langlois J. M. Pierre. Red Lesion Detection Using Dynamic Shape Features for Diabetic Retinopathy Screening *IEEE Trans. Med. Imaging.* 2016;35:1116–1126.

[4] Dashtbozorg B., Zhang J., Huang ., Haar Romeny B. M.. Retinal Microaneurysms Detection Using Local Convergence Index Features *IEEE Trans. Image Processing.* 2018;27:3300–3315.

[5] Pires R., Avila S., Jelinek H. F., Wainer J., Valle E., Rocha A.. Beyond Lesion-Based Diabetic Retinopathy: A Direct Approach for Referral *IEEE J. Biomed. Health.* 2017;21:193–200.

[6] Shen X., Wu Y.. A unified approach to salient object detection via low rank matrix recovery in *Proceedings of CVPR*:853–860 2012.

[7] Itti L., Koch C., Niebur E.. A model of Saliency-Based visual attention for rapid scene analysis *IEEE Trans. on Pattern Anal. Mach.Intell.*. 1998;20:1254-1259.

[8] Koch C., Ullman S.. Shifts in selective visual attention: towards the underlying neural circuitry. *Human neurobiology.* 1985;4 4:219-27.

[9] Yuan Y., Wang J., Li B., Meng M.. Saliency Based Ulcer Detection for Wireless Capsule Endoscopy Diagnosis *IEEE Trans. Med. Imaging.* 2015;34:2046–2057.

[10] Yan J., Zhu M., Liu Y.. Visual Saliency Detection via Sparsity Pursuit *IEEE Signal Process. Lett..* 2010;17:739–742.

[11] Ko B., Nam J.. Object-of-interest image segmentation based on human attention and semantic region clustering *J. Opt. Soc. Am. A.* 2006;23:2462-2470.

[12] Zhao Y., Zheng Y., Zhao Y., et al. Uniqueness-Driven Saliency Analysis For Automated Abnormalities Detection with Application to Retinal Diseases in *Proceedings of MICCAI*:109-118 2018.

[13] Roychowdhury S., Parhi K.K.. DREAM: Diabetic Retinopathy Analysis Using Machine Learning *IEEE J. Biomed. Health.* 2014;18:1717–1728.

[14] Mansour R. F.. Evolutionary Computing Enriched Computer-Aided Diagnosis System for Diabetic Retinopathy: A Survey *IEEE Reviews in Biomed. Eng..* 2017;10:334-349.

[15] Fleming A. D., Philip S., Goatman K. A., Olson J.A., Sharp P. F.. Automated microaneurysm detection using local contrast normalization and local vessel detection *IEEE Trans. Med. Imaging.* 2006;25:1223–1232.

[16] Giancardo L., Mériaudeau F., Li Y., Tobin K. W., Chaum E.. Microaneurysm detection with radon transform-based classification on retina images in *Proceedings of EMBC*:5939–5942 2011.

[17] Tang L., Niemeijer M., Reinhardt J. M., Garvin M. K., Abràmoff M. D.. Splat Feature Classification With Application to Retinal Hemorrhage Detection in Fundus Images *IEEE Trans. Med. Imaging.* 2013;32:364–375.

[18] Pereira C., Gonçalves L., Ferreira M.. Exudate Segmentation in Fundus Images Using an Ant Colony Optimization Approach *Inf. Sci..* 2015;296:14–24.

[19] Dai B., Wu X., Bu W.. Retinal microaneurysms detection using gradient vector analysis and class imbalance classification *PLOS ONE.* 2016;11:1-23.

[20] Phillips R., Forrester J., Sharp P.. Automated detection and quantification of retinal exudates *Graefes Arch Clin Exp Ophthalmol..* 1993;231:90-4.

[21] Walter T., Klein J., Massin P., Erginay A.. A contribution of image processing to the diagnosis of diabetic retinopathy-detection of exudates in color fundus images of the human retina *IEEE Trans. Med. Imaging.* 2002;21:1236-1243.

[22] Sánchez C. I., García M., Mayo A., López M. Isabel, Hornero R.. Retinal image analysis based on mixture models to detect hard exudates *Med. image anal..* 2009;13 4:650-8.

[23] Sánchez C. I., Niemeijer M., Isgum I., et al. Contextual computer-aided detection: Improving bright lesion detection in retinal images and coronary calcification identification in CT scans *Med. image anal..* 2012;16 1:50-62.

[24] Welfer D., Scharcanski J., Marinho D.. A coarse-to-fine strategy for automatically detecting exudates in color eye fundus images *Comp. Med. Imag. and Grap..* 2010;34:228-35.

[25] Giancardo L., al. . Exudate-based diabetic macular edema detection in fundus images using publicly available datasets *Med. Image Anal..* 2012;16:216–226.

[26] Agurto C., Murray V., Yu H., et al. A Multiscale Optimization Approach to Detect Exudates in the Macula *IEEE J. Biomed. Health.* 2014;18:1328–1336.

[27] Rabbani H., Allingham M., Farsiu S.. Fully automatic segmentation of fluorescein leakage in subjects with diabetic macular edema *Invest. Ophthalmol. Vis. Sci..* 2015;56:1482-1492.

[28] Zhao Y., Zheng Y., Liu Y., et al. Intensity and Compactness Enabled Saliency Estimation for Leakage Detection in Diabetic and Malarial Retinopathy *IEEE Trans. Med. Imaging.* 2017;36:51–63.

[29] Liu Q., Zhou B., Ke W., Zhao G.. A location-to-segmentation strategy for automatic exudate segmentation in colour retinal fundus images *Comp. Med. Imag. and Grap..* 2017;55:78–86.

[30] Rocha A., Carvalho T., Jelinek H. F., Goldenstein S., Wainer J.. Points of Interest and Visual Dictionaries for Automatic Retinal Lesion Detection *IEEE Trans. Biomed. Eng..* 2012;59:2244-2253.

[31] Zhang X., Thibault G., Decencière E., et al. Exudate detection in color retinal images for mass screening of diabetic retinopathy *Med. Image Anal..* 2014;18 7:1026-43.

[32] Gondal W. M., Köhler J. M., Grzeszick R., Fink G. A., Hirsch M.. Weakly-supervised localization of diabetic retinopathy lesions in retinal fundus images *Proceedings of ICIP.* 2017:2069-2073.

[33] Quellec G., Charrière K., Y.Boudi , Cochener B., Lamard M.. Deep image mining for diabetic retinopathy screening *Med. Image Anal..* 2017;39:178–193.

[34] Perazzi F., Pritch Y., Hornung A.. Saliency filters: Contrast based filtering for salient region detection in *Proceedings of CVPR* 2012.

[35] Cheng M., Zhang G., Mitra N., , Hu S.. Global Contrast based Salient Region Detection in *Proceedings of CVPR*:409-416 2011.

[36] Achanta R., Shaji A., Smith K., Lucchi A., Fua P.. SLIC Superpixels Compared to State-of-the-art Superpixel Methods *IEEE Trans. Pattern Anal. Mach.Intell..* 2012;34:2274-2282.

[37] Candès E. J., Li X., Ma Y., Wright J.. Robust Principal Component Analysis? *J. ACM.* 2011;58:11:1–11:37.

[38] Wright J., Ganesh A., Rao S., Peng Y., Ma Y.. Robust Principal Component Analysis: Exact Recovery of Corrupted Low-Rank Matrices via Convex Optimization in *Proceedings of NIPS*:2080–2088 2009.

[39] Zhao Y., Rada L., Chen K., Harding S., Zheng Y.. Automated vessel segmentation using infinite perimeter active contour model with hybrid region information with application *IEEE Trans. Med. Imaging.* 2015;34:1797-1807.

[40] Li C., Xu C., Gui C., Fox M. D.. Distance Regularized Level Set Evolution and Its Application to Image Segmentation *IEEE Transactions on Image Processing.* 2010;19:3243-3254.

[41] Zhao Y., MacCormick I. J., Beare N., Harding S. P., Zheng Y.. Automated Detection of Leakage in Fluorescein Angiography Images with Application to Malarial Retinopathy *Sci. Rep..* 2015;5:e10425.

[42] Cheng J., al. . Superpixel Classification Based Optic Disc and Optic Cup Segmentation for Glaucoma Screening *IEEE Trans. Med. Imaging.* 2013;32:1019-1032.

[43] Tobin K.W., Chaum E., Govindasamy V., Karnowski T.. Detection of anatomic structures in human retinal imagery *IEEE Trans. on Med. Imag..* 2014;26:1729-1739.

[44] Akram M. Usman, Tariq Anam, Khan Shoab A., Javed M. Younus. Automated Detection of Exudates and Macula for Grading of Diabetic Macular Edema *Comput. Methods Prog. Biomed..* 2014;114:141–152.

[45] Kauppi T., Kalesnykiene V., Sorri I., et al. The DIARETDB1 Diabetic Retinopathy Database and Evaluation Protocol in *Proceedings of BMVC* 2007.

[46] Niemeijer M., Ginneken B., M. D. Abramoff et al.. Retinopathy Online Challenge: Automatic Detection of Microaneurysms in Digital Color Fundus Photographs *IEEE Trans. Med. Imaging.* 2010;29:185–195.

[47] Decencire E., al. . TeleOphta: Machine learning and image processing methods for teleophthalmology *IRBM.* 2013;34:196–203.

[48] Kandemir M., Hamprecht F. A.. Computer-aided diagnosis from weak supervision: A benchmarking study *Comput. Med. Imag. Grap..* 2015;42:44-50.

[49] Antal B., al. . An Ensemble-Based System for Microaneurysm Detection and Diabetic Retinopathy Grading *IEEE Trans. Biomed. Eng..* 2012;59:1720–1726.

[50] Wu B., Zhu W., Shi F., Zhu S., Chen X.. Automatic detection of microaneurysms in retinal fundus images *Comp. Med. Imag. and Grap..* 2017;55:106–112.

[51] Wang S, Tang H, al. . Localizing Microaneurysms in Fundus Images Through Singular Spectrum Analysis *IEEE Trans. Biomed. Eng..* 2017;64:990-1002.

[52] Zhou L., al. . Automatic hemorrhage detection in color fundus images based on gradual removal of vascular branches in *Proceedings of ICIP*:399-403 2016.

[53] Haloi M., Dandapat S., Sinha R.. A Gaussian Scale Space Approach For Exudates Detection, Classification And Severity Prediction *CoRR.* 2015;abs/1505.00737.

[54] Hou X., Zhang L.. Saliency detection: A spectral residual approach. in *Proceedings of CVPR*:1-8 2007.

[55] Achanta R., Hemami S., Estrada F., Susstrunk S.. Frequency-tuned salient region detection in *Proceedings of CVPR*:1597-1604 2009.

[56] Harel J., Koch C., Perona. P.. Graph-based visual saliency in *Proceedings of NIPS*:545-552 2006.

[57] Goferman S., Zelnik-Manor L., Tal A.. Context-Aware Saliency Detection *IEEE Trans. Pattern Anal. Machine Intell..* 2012;34:1915–1926.